International Journal of Engineering Trends and Technology
ISSN: 2231–5381 / https://doi.org/10.14445/22315381/IJETT-V73I7P120

Volume 73 Issue 7, 254-268, July 2025

Original Article

Numerical Analysis of the Effect of Baffles on Improving the Performance of a Hybrid Photovoltaic / Thermal Flat-Plate Air Solar Collector

Yao Kombate[1*], Kokou N'wuitcha[1,2], Yendouban Kolani[2], Komlan Déla Donald Aoukou[2], Koffi Gagnon Apedanou[2], Bernard Obese[3]

[1]*Regional Center of Excellence for Electricity Control (CERME), University of Lomé (UL), Lomé, Togo.*
[2]*Solar Energy Laboratory, Department of Physics, Faculty of Sciences, University of Lomé (UL), Lomé, Togo.*
[3]*Department of Science Education, University of Cape Coast, Cape Coast, Ghana.*

[*]*Corresponding Author: kyao2120@gmail.com*

Received: 22 February 2025 Revised: 21 May 2025 Accepted: 16 June 2025 Published: 30 July 2025

Abstract - *The hybrid photovoltaic/thermal (PVT) solar collector is a cogeneration system that produces electricity and heat simultaneously. The performance of the hybrid photovoltaic/thermal air solar collector is limited by the low convection heat transfer coefficient between the absorber plate and the air in circulation. The addition of baffles in the air duct improves the coefficient and therefore the performance of the hybrid photovoltaic/thermal solar collector. The performance of the hybrid photovoltaic-thermal air collector is affected by the layout and shape of the baffles. In this study, a two-dimensional dynamic regime thermal model was developed to evaluate the performance of two distinct photovoltaic solar configurations: an air-cooled flat-plate hybrid photovoltaic-thermal solar collector and an air-cooled flat-plate hybrid photovoltaic-thermal solar collector with rectangular baffles, in order to investigate the effect of cooling on the solar photovoltaic module. All the mathematical equations obtained were discretised using the finite difference method. The implicit alternating directions scheme was used for the heat transfer equations within the fluid. The resulting system of algebraic equations is solved using Thomas' algorithm in the FORTRAN environment. The model is validated by comparing the numerical and experimental results from the literature. The results showed that the maximum electrical efficiency of the photovoltaic module increased from 13.04% to 14.39% for the air-cooled PVT hybrid collector without baffles and from 13.04% to 14.74% for the air-cooled PVT hybrid collector with baffles. This represents an increase of 1.70% in electrical efficiency, an average gain of 40.18% in thermal efficiency, an overall exergy of 16.90% and an entropy of 1.60 W/K. The numerical results provide valuable insight into optimizing the design and operating conditions.*

Keywords - *Hybrid photovoltaic/thermal solar collector, Modelling, Electrical efficiency, Thermal efficiency, Baffles, Exergy.*

1. Introduction

Countries around the world depend mainly on fossil fuels (coal, oil and natural gas) to meet their energy needs. Available in limited quantities, these fossil fuel sources are being depleted at an accelerating rate. Their massive use is contributing to global warming by releasing carbon dioxide into the atmosphere. To meet energy needs and solve environmental problems, renewable energies are an alternative to fossil fuels. Electrical and thermal energy, produced by photovoltaic (PV) solar modules and thermal solar collectors, respectively, are the two forms of energy obtained from solar energy [1]. Made from semiconductor materials, mainly silicon, PV solar modules convert solar radiation directly into electricity [2]. When these PV solar cells absorb solar radiation, unwanted heat is generated, leading to an increase in their temperature and, consequently, a decrease in electrical efficiency [3, 4]. To improve the electrical efficiency of solar PV modules, it is necessary to cool them by converting undesirable heat into useful heat for residential and industrial applications [5, 6].

2. Literature Review

In recent years, research has been carried out into methods of cooling solar PV modules. One of the methods of cooling PV solar modules is the forced circulation of air at the back of the PV solar module. This active method highlights the design of a new solar technology called hybrid photovoltaic/thermal (PVT) solar collectors, which produce electricity and heat from solar radiation. It extracts undesired heat from the PV module and keeps its electrical efficiency constant by increasing the air mass flow rate. A comparative study of the performance of four different configurations of

hybrid air collectors under the same climatic conditions by Srimanickam et al. [7] showed that the electrical efficiency increased from 9.8% to 12.9% for an air mass flow rate of 0.00847 kg/s and from 10.3% to 13.9% for an air mass flow rate of 0.0113 kg/s. The thermal efficiency was respectively between 4.3% and 12.4% for an air mass flow rate of 0.00847 kg/s and between 6.5% and 15.9% for an air mass flow rate of 0.0113 kg/s. [7] Omer and Zala [8] showed that the electrical efficiency and thermal efficiency of the hybrid PVT collector increased by 20% and 44%, respectively, when the air flow rate was increased from 0.024 to 0.057 m^3/s. Tripty and Nasrin [9] developed a three-dimensional (3D) model of a hybrid PVT air collector and analysed the behaviour of the system consisting of six aluminium sheets (1 mm thick fins) inside the heat exchanger. The results indicated a thermal energy output of 302 W to 514 W for a flow rate of 0.015 to 0.535 kg/s. For an increase of 0.097 kg/s, thermal energy and electrical power increased by 42.4 W and 1.596 W, respectively, while output and PV solar cell temperatures decreased by 3.796 °C and 3.8 °C, respectively. Thermal, electrical and overall efficiencies are improved by 6.994%, 6.738% and 0.256% when the mass flow rate is increased by 0.097 kg/s. An experimental study by Ganesan et al. [10] showed that natural convection cooling methods improved the electrical efficiency of the PV module by 27.7% when its temperature was reduced by 17.3%. Basem et al. [11] showed that air cooling in a channel, water cooling in the tubes and aluminium oxide-water nanofluid cooling in the tubes behind the PV module improved the electrical efficiency by 1.1%, 1.9% and 2.7% respectively. This study showed that air cooling is less efficient than the other two cooling methods used. This limited cooling method is due to the low thermal capacity, conductivity and heat transfer coefficient. To improve these thermophysical properties of the air, barriers are added to the air duct at the rear of the solar PV module.

Optimising the structural configuration of the airflow channels improves heat transfer and reduces the temperature of the PV modules. Indeed, an experimental study by Alshibil et al. [12] showed that the thermal efficiency of the hybrid PVT collector with louvred fins increased by 48% and 54% compared with the hybrid PVT collector with vertical fins and the hybrid PVT collector without fins, respectively. Thus, louvred fins were more efficient for the same surface area than vertical fins. Zhang et al. [13] designed a hybrid PVT air collector using fins with double-layer flow channels, with the upper channel equipped with transparent corrugated plates and the lower channel with offset fins. The results showed that the maximum overall efficiency was 56.261% when the height of the upper and lower fins was 23 mm and 105 mm, for an equivalent diameter of 70 mm and three (03) fins. The average overall yield increased by 8.21% compared to other collectors under the same conditions. Different innovative hybrid PVT collector configurations with convex flow channel wall shapes such as hemispheres, cylinders, cones and cuboids were investigated by Wang et al. [14]. Compared with the conical shape, the cylindrical shape showed improvements in electrical and thermal efficiency of 1.73% and 8.29%, respectively. In addition, the electrical and thermal powers increased by 2.1675 W and 59.19 W with the cylindrical configuration. Kim et al. [15] conducted a comparative study of three hybrid PVT air collector configurations: a hybrid PVT air collector with longitudinal fins and rectangular turbulators, a hybrid PVT air collector with a smooth channel and a hybrid PVT air collector with fins only.

The results showed that the hybrid PVT air collector with longitudinal fins and rectangular turbulators achieved an electrical efficiency of 17.06%, while the hybrid PVT air collector with a smooth channel and the hybrid PVT air collector with fins gave corresponding values of 16.55% and 16.8%, respectively. In addition, the hybrid PVT air collector with longitudinal fins and turbulators achieved a thermal efficiency of 38.93%, while the hybrid PVT air collector with a smooth channel and the hybrid PVT air collector with fins achieved thermal efficiencies of 22.68% and 33.56% respectively. Genge et al. [16] investigated the impact of the number of fins on the PV panel surface temperature and on the air flow in the collector-fan cavity. The numerical results indicated that increasing the number of fins to 34 decreased the surface temperature of the solar PV panel from 65°C to 50.99°C, a reduction of 14.1°C. Bayrak et al. [17] experimentally investigated the effects of passive cooling on the temperature, power output and energy-energy efficiencies of solar PV panels for ten (10) different fin configurations. It was observed that the temperature was not evenly distributed over the surface of the PV panel. The highest energy and exergy efficiency of the PV panels, 11.55% and 10.91% respectively, were obtained with the finned configuration (named A5).

Various configurations of obstacles used in airflow channels for cooling PV modules have been proposed in the literature. Rectangular, triangular, inclined, perforated, curved and then V-shaped and T-shaped baffles were used as obstacles in the air ducts to improve the performance of the solar PV module. With perforated baffles, the total exergy efficiency of the hybrid PVT air collector with perforated baffles was 24.8% to 30.5% while the total energy efficiency was 44.1% to 63.3% [18]. When using the curved baffles, thermal efficiency and electrical efficiency were 37.1% and 6.4%, respectively. In addition, annual thermal energy and electric energy produced were 644 kWh and 118 kWh, respectively [19]. When triangular obstacles were used in the air duct of a hybrid PVT collector, the average daily thermal, electrical, energy and exergy efficiencies were 24.73%, 15.59%, 62.83% and 15.57%, respectively. On the other hand, for a PVT hybrid air collector without triangular obstacles, these efficiencies were 17.08%, 15.30%, 54.47% and 15.13%, respectively [20]. According to the same authors, the energy and exergy of the hybrid PVT collector with triangular obstacles produced annually were 12.84% and 1.98% greater

than those of the hybrid PVT collector without obstacles. Another experimental study by Yu et al. [21] showed that the use of triangular baffles increased the air outlet temperature by 3.6 °C to 3.9°C and the useful heat by 1.28 to 1.31 times compared to the hybrid PVT solar collector without baffles. As a result, the PVT air hybrid solar collector with baffles saw thermal efficiency increased by 31%, maximum output speed increased by 1.03 times and mean Reynolds number increased by 1.05 times. Srimanickam and Sarayan [22] showed that the coupling of fins to V-shaped baffles had the highest electrical and thermal performance compared with the other configurations because of its physical geometry, which is rich in artificial roughness. Zine et al. [23] experimentally evaluated and compared the electrical and thermal performance of a hybrid PVT collector with baffles and a hybrid PVT collector without baffles. The results showed that the thermal and electrical efficiencies of the hybrid PVT collector were on average 86% and 9%, respectively. This results in a 22% improvement over a hybrid PVT collector without baffle fixation in the absorber.

The integration and combination of cooling methods for solar PV modules should be implemented to improve both the heat transfer surface area and the heat transfer coefficient. These heat transfer characteristics can be limited by the shape of the baffles and stagnation zones. To increase heat transfer and reduce hot air stagnation zones, a simple shape and regular arrangement of the baffles lengthens the air flow in the duct and improves the performance of the flat-plate hybrid PVT air collector. In addition, most studies in the literature have used steady-state thermal models to numerically determine the performance of the hybrid flat plate air collector. Such an operating regime does not take into account fluid flow in all directions, which may lead to an overestimation or underestimation of the performance of the flat-plate hybrid PVT air collector under varying climatic conditions.

Two-dimensional (2D) dynamic thermal models with laminar airflow in the duct of the flat-plate PVT air hybrid solar collector are often not taken into account when determining temperature distribution and performance. In this study, rectangular-shaped baffles were installed in the airflow channel of the hybrid flat-plate PVT solar collector. The main objective is to investigate the effect of adding baffles in the airflow channel on the performance of the hybrid flat-plate PVT solar collector. To this effect, a 2D dynamic thermal model has been developed in order to numerically compare the electrical and thermal performance of the flat-plate hybrid PVT solar collector with and without baffles.

3. Materials and Methods

3.1. Physical Model and Assumptions

The physical model of the system studied was a hybrid PVT flat-plate solar air collector consisting of the PV solar module and a heat exchanger, shown in Figure 1. It consists of three (03) main parts:

- The part creating the greenhouse effect consists of a layer of air confined between the glass cover and the upper protective glass of the PV solar cells.
- The PV module part consists of three essential solid layers:
  - A layer of top protective glass;
  - PV solar cells immersed in an Ethylene-vinyl acetate (EVA) polymer layer;
  - A lower protective glass layer.
- The heat exchanger section consists of three layers:
  - An absorber plate behind the glass; this is a corrosion-resistant stainless-steel sheet.
  - a rectangular air duct or air flow channel to convey the useful heat;
  - An insulation to minimise heat loss to the sides and rear of the hybrid PVT collector's air duct.

With the reference hybrid PVT collector, single rectangular baffles were fitted in the air duct to guide the direction of airflow (see Figure 2). Six (06) simple rectangular baffles were fixed in the path of the airflow. The laminar flow is incompressible, two-dimensional and dynamic with no internal heat generation and negligible viscous dissipation. The thermophysical properties of air vary according to its temperature, but those of the solid layers are constant. The air flow is modelled by the Navier-Stokes equations, and the heat transfer equations between the solid layers of the collector by the first law of thermodynamics. The side walls of the hybrid PVT collector were considered to be adiabatic. The change in density in the air that leads to natural convection is considered only in terms of body forces in the Boussinesq approximation.

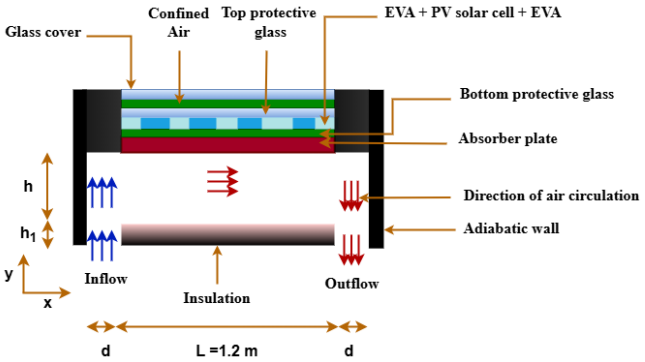

Fig. 1 Cross-section of a flat-plate hybrid PVT air collector

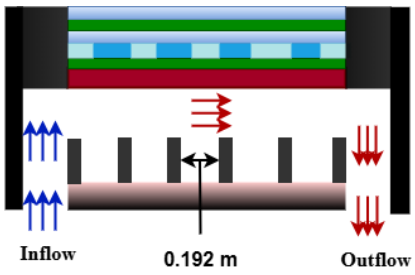

Fig. 2 Cross-section of a hybrid PVT air collector with baffles

Thus, buoyancy forces of equation 1 created by both temperature and specific vapour density of air gradient are taken into account in the momentum equation [24].

$$\vec{f} = g(sin\gamma.\vec{\imath} + cos\gamma.\vec{j})[\beta_T(T - T_\infty) + \beta_c(c - c_\infty)] \quad (1)$$

With g, the gravity intensity,$\beta_T$the volumetric coefficient of thermal expansion and$\beta_c$the coefficient of expansion specified for air are approximated on the basis of the reference temperature $T_\infty$and the reference concentrationc_∞.

The governing equations of the fluid were put into dimensionless form by introducing the transformations given by equations 2 and 3.

$$X = \frac{x}{L};\ Y = \frac{y}{L};\ U_f = \frac{u_f}{V_0};\ V_f = \frac{v_f}{V_0};\ \tau = \frac{V_0\ t}{L} \quad (2)$$

$$\theta = \frac{T_f - T_a}{T_{fe} - T_a};\ C = \frac{c_f - c_a}{c_{fe} - c_a}; \Omega_f = \frac{\omega_f L}{V_0}\ ; \Psi_f = \frac{\psi_f}{LV_0} \quad (3)$$

3.2. Basic Mathematical Equations in the Fluid Zone and Boundary Conditions

Taking into account the physical model and the assumptions made with dimensionless variables in equations 2 and 3, we obtained the non-dimensional fluid equations.

(a) Vorticity, current flow and velocity field equations:

$$\frac{\partial \Omega_f}{\partial \tau} + U_f \frac{\partial \Omega_f}{\partial X} + V_f \frac{\partial \Omega_f}{\partial Y} = \frac{1}{R_e}\left(\frac{\partial^2 \Omega_f}{\partial X^2} + \frac{\partial^2 \Omega_f}{\partial Y^2}\right)$$

$$+R_{iT}\left[cos\gamma \frac{\partial \theta_f}{\partial X} - sin\gamma \frac{\partial \theta_f}{\partial Y}\right] + R_{ic}\left[cos\gamma \frac{\partial C_f}{\partial X} - sin\gamma \frac{\partial C_f}{\partial Y}\right] \quad (4)$$

$$\Omega_f = -\left(\frac{\partial^2 \Psi_f}{\partial X^2} + \frac{\partial^2 \Psi_f}{\partial Y^2}\right) \quad (5)$$

$$\Omega = \frac{\partial V_f}{\partial X} - \frac{\partial U_f}{\partial Y}\ \ ;\ \ U_f = \frac{\partial \Psi_f}{\partial Y}\ \ ;\ \ V_f = -\frac{\partial \Psi_f}{\partial X} \quad (6)$$

(b) Energy equation in the fluid:

$$\frac{\partial \theta_f}{\partial \tau} + U_f \frac{\partial \theta_f}{\partial X} + V_f \frac{\partial \theta_f}{\partial Y} = \frac{1}{R_e \times P_r}\left(\frac{\partial^2 \theta_f}{\partial X^2} + \frac{\partial^2 \theta_f}{\partial Y^2}\right) \quad (7)$$

(c) Humidity diffusion equation:

$$\frac{\partial C_f}{\partial \tau} + U_f \frac{\partial C_f}{\partial X} + V_f \frac{\partial C_f}{\partial Y} = \frac{1}{S_c \times R_e}\left(\frac{\partial^2 C_f}{\partial X^2} + \frac{\partial^2 C_f}{\partial Y^2}\right) \quad (8)$$

The boundary conditions:

(a) At the initial date: $(\tau = \tau_0)$

$$U_f = V_f = 0,\ \Omega_f = 0,\ \Psi_f = 0,\ \theta_f = 0,\ C_f = 0 \quad (9)$$

(b) at the airflow channel: $(0 \prec X \prec \frac{d}{L}; Y = 0)$

$$U_f = 0\ ; V_f = 1\ ; \Psi_f = -X\ ; \theta_f = 0\ ; C_f = 0$$

$$\Omega_f = -\left.\frac{\partial^2 \Psi_f}{\partial Y^2}\right|_{X,Y=0} \quad (10)$$

(c) at the airflow channel outlet: $(1 - \frac{d}{L} \prec X \prec 1\ ; Y = 0)$

$$\left.\frac{\partial U_f}{\partial Y}\right|_{X,Y=0} = \left.\frac{\partial\ V_f}{\partial Y}\right|_{X,Y=0} = 0\ ;\ \left.\frac{\partial \theta_f}{\partial Y}\right|_{X,Y=0} = 0$$

$$\left.\frac{\partial C_f}{\partial Y}\right|_{X,Y=0} = 0\ ; \left.\frac{\partial \Psi_f}{\partial Y}\right|_{X,Y=0} = 0; \left.\frac{\partial \Omega_f}{\partial Y}\right|_{X,Y=0} = 0 \quad (11)$$

(d) At the inside walls of the air duct:

- Adiabatic wall at the air duct inlet:

$(X = 0; 0 \prec Y \prec \frac{H}{L})$

$$U_f = V_f = 0\ ;\ \left.\frac{\partial \theta_f}{\partial X}\right|_{X=0,Y} = 0\ ;\ \left.\frac{\partial C_f}{\partial X}\right|_{X=0,Y} = 0$$
$$\Psi_f = 0\ ; \Omega_f = -\left.\frac{\partial^2 \Psi_f}{\partial X^2}\right|_{X=0,Y} \quad (12)$$

- Insulation wall at the entrance of the duct:

$(X = \frac{d}{L}; 0 \prec Y \prec \frac{H_1}{L})$

$$U_f = V_f = 0\ ;\ \left.\frac{\partial \theta_f}{\partial X}\right|_{X=\frac{d}{L},Y} = 0\ ;\ \left.\frac{\partial C_f}{\partial X}\right|_{X=\frac{d}{L},Y} = 0$$
$$\Psi_f = -\frac{d}{L}\ ; \Omega_f = -\left.\frac{\partial^2 \Psi_f}{\partial X^2}\right|_{X=\frac{d}{L},Y} \quad (13)$$

- Insulation part at the outlet of the conduit:

$(X = 1 - \frac{d}{L}; 0 \prec Y \prec \frac{H_1}{L})$

$$U_f = V_f = 0\ ;\ \left.\frac{\partial \theta_f}{\partial X}\right|_{X=1-\frac{d}{L},Y} = 0\ ; \Psi_f = -\frac{d}{L}$$
$$\left.\frac{\partial C_f}{\partial X}\right|_{X=1-\frac{d}{L},Y} = 0\ ;\ \Omega_f = -\left.\frac{\partial^2 \Psi_f}{\partial X^2}\right|_{X=1-\frac{d}{L},Y} \quad (14)$$

- Adiabatic wall at the outlet of the duct:

$(X = 1; 0 \prec Y \prec \frac{H}{L})$

$$U_f = V_f = 0\ ; \left.\frac{\partial \theta_f}{\partial X}\right|_{X=1,Y} = 0\ ; \left.\frac{\partial C_f}{\partial X}\right|_{X=1,Y} = 0$$

$$\Psi_f = 0\ ;\ \Omega_f = -\left.\frac{\partial^2 \Psi_f}{\partial X^2}\right|_{X=1,Y} \quad (15)$$

- Bottom-air heat exchanger wall interface:

$(\frac{d}{L} \prec X \prec 1 - \frac{d}{L}; Y = \frac{H_1}{L})$

$$U_f = V_f = 0\ ;\ \theta_f = \theta_{ins}\ ; \left.\frac{\partial C_f}{\partial Y}\right|_{X,Y=\frac{H_1}{L}} = 0$$
$$\Psi_f = -\frac{d}{L};\ \Omega_f = -\left.\frac{\partial^2 \Psi_f}{\partial Y^2}\right|_{X,Y=\frac{H_1}{L}} \quad (16)$$

- Upper-air heat exchanger interface wall: $(0 \prec X \prec 1; Y = \frac{H}{L})$

$$U_f = V_f = 0;\ \Psi_f = 0;\ \Omega_f = -\left.\frac{\partial^2 \Psi_f}{\partial Y^2}\right|_{X,Y=\frac{H}{L}}$$
$$\theta_f = \theta_p\ ; \left.\frac{\partial C_f}{\partial Y}\right|_{X,Y=\frac{H}{L}} = 0 \quad (17)$$

With:

x, y: cartesian coordinate axes (m); X, Y: dimensionless coordinate axes ; u_f, v_f: components of the fluid velocity vectors in the x and y directions $(m.s^{-1})$;U_f, V_f: dimensionless velocities in the x and y directions respectively ; c_f: mass fraction of the air vapor or moisture (kg water/kg dry air); c_{fe}: fluid moisture near the plate (kg water/kg dry air) ; c_a: concentration in the fluid away from the plate (kg water/kg dry air); : dimensionless concentration; T_f: temperature of the plate (°C) ; T_{fe}: temperature of the fluid near the plate (°C);T_a: temperature of the fluid far from the plate (°C); θ_f: temperature of the fluid dimensionless; t:time (s) ; τ:time dimensionless;ω_f: vorticity function;ψ_f: air stream lines; Ω_f: dimensionless vorticity function; Ψ_f: dimensionless air stream lines;: angle of inclination of the hybrid solar collector PVT with respect to horizontal (°C); $R_e = \frac{\rho_f L V_0}{\mu_f}$: the number of Reynolds;$P_r = \frac{\mu C_p}{\lambda}$:the number of Prandtl ; $R_{i_T} = \frac{g\beta_T L \Delta T}{{V_0}^2}$: the Richardson number related to temperature; $R_{i_C} = \frac{g\beta_c L \Delta c}{{V_0}^2}$: the Richardson number related to humidity; $Sc = \frac{\nu}{D}$: the Schmidt number.

3.3. Basic Equations in the Solid Layers

The energy balance in the various solid layers of the PVT hybrid collector is determined by the following equations:

(a) Energy equation for the glass cover:

$$\rho_g e_g C_g \frac{\partial T_g}{\partial t} = \alpha_g G - h^{ray}_{g-ciel}\left(T_g - T_{ciel}\right) - h^{ray}_{g-g_1}\left(T_g - T_{g_1}\right) - h^{conv}_{g-amb}\left(T_g - T_{amb}\right) - h^{conv}_{g-cf}\left(T_g - T_{cf}\right) + \lambda_g e_g \left(\frac{\partial^2 T_g}{\partial x^2} + \frac{\partial^2 T_g}{\partial y^2}\right) \quad (18)$$

(b) Energy equation for confined air:

$$\rho_{cf} e_{cf} C_{cf} \frac{\partial T_{cf}}{\partial t} = -h^{cv}_{cf-g}\left(T_{cf} - T_g\right) - h^{cv}_{cf-g_1}\left(T_{cf} - T_{g_1}\right) + \lambda_{cf} e_{cf} \left(\frac{\partial^2 T_{cf}}{\partial x^2} + \frac{\partial^2 T_{cf}}{\partial y^2}\right) \quad (19)$$

(c) Upper glass (glass 1) energy equation:

$$\rho_{g_1} e_{g_1} C_{g_1} \frac{\partial T_{g_1}}{\partial t} = \alpha_g \tau_g G - h^{rd}_{g_1-v}\left(T_{g_1} - T_g\right) - h^{cv}_{g_1-cf}\left(T_{g_1} - T_{cf}\right) - h^{cd}_{g_1-pv}\left(T_{g_1} - T_{pv}\right) + \lambda_{g_1} e_{g_1} \left(\frac{\partial^2 T_{g_1}}{\partial x^2} + \frac{\partial^2 T_{g_1}}{\partial y^2}\right) \quad (20)$$

(d) PV solar cell energy equation:

$$\rho_{pv} e_{pv} C_{pv} \frac{\partial T_{pv}}{\partial t} = \alpha_{pv} \tau_g^2 \beta G\ - h^{cd}_{pv-g_1}\left(T_{pv} - T_{g_1}\right) - h^{cd}_{pv-g_2}\left(T_{pv} - T_{g_2}\right) + \lambda_{pv} e_{pv} \left(\frac{\partial^2 T_{pv}}{\partial x^2} + \frac{\partial^2 T_{pv}}{\partial y^2}\right) \quad (21)$$

(e) Lower glass (glass 2) energy equation:

$$\rho_{g_2} e_{g_2} C_{g_2} \frac{\partial T_{g_2}}{\partial t} = -h^{cd}_{pv-g_2}\left(T_{g_2} - T_{pv}\right) - h^{cd}_{v_2-p}\left(T_{g_2} - T_p\right) + \lambda_{g_2} e_{g_2} \left(\frac{\partial^2 T_{g_2}}{\partial x^2} + \frac{\partial^2 T_{g_2}}{\partial y^2}\right) \quad (22)$$

(f) Energy equation of the absorber plate:

$$\rho_p e_p C_p \frac{\partial T_p}{\partial t} = h^{cv}_{p-f}\left(T_p - T_f\right) - h^{cd}_{g_2-p}\left(T_p - T_{g_2}\right) - h^{rd}_{p-ins}\left(T_p - T_{ins}\right) + \lambda_p e_p \left(\frac{\partial^2 T_p}{\partial x^2} + \frac{\partial^2 T_p}{\partial y^2}\right) \quad (23)$$

(g) Energy equation of the insulation layer:

$$\rho_{ins} e_{ins} C_{ins} \frac{\partial T_{ins}}{\partial t} = -h^{rd}_{p-ins}\left(T_p - T_{ins}\right) - h^{cv}_{ins-amb}\left(T_{ins} - T_{amb}\right) - h^{rd}_{ins-sol}\left(T_{ins} - T_{gr}\right) + \lambda_{ins} e_{ins} \left(\frac{\partial^2 T_{ins}}{\partial x^2} + \frac{\partial^2 T_{ins}}{\partial y^2}\right) \quad (24)$$

The heat transfer correlation coefficients used are [25-27]:

- Coefficient of heat transfer by radiation between the glass cover and the sky.

$$h^{rd}_{g-sky} = \varepsilon_g \sigma \left(T_g^2 + T_{sky}^2\right)\left(T_g + T_{sky}\right) \quad (25)$$

Where$\sigma = 5.67.10^{-8} W/m^2.K^4$ the sky temperature was calculated using Swinbank's formula.

$$T_{sky} = 0.0522 \times T_{amb}^{1,5} \quad (26)$$

- Coefficient of radiation heat transfer between insulation and soil.

$$h^{rd}_{ins-gr} = \frac{\sigma\left(T_{ins}^2 + T_{gr}^2\right)\left(T_{ins} + T_{gr}\right)}{\frac{1}{\varepsilon_{ins}} + \frac{1}{\varepsilon_{gr}} - 1} \quad (27)$$

- Coefficient of radiation heat transfer between the glass cover and the top protective glass.

$$h_{g-g_1}^{rd} = \frac{\sigma(T_g^2+T_{g_1}^2)(T_g+T_{g_1})}{\frac{1}{\varepsilon_g}+\frac{1}{\varepsilon_{g_1}}-1} \quad (28)$$

- Coefficient of heat transfer by radiation between the absorbing plate and the insolation.

$$h_{p-ins}^{rd} = \frac{\sigma(T_p^2+T_{ins}^2)(T_p+T_{ins})}{\frac{1}{\varepsilon_p}+\frac{1}{\varepsilon_{ins}}-1} \quad (29)$$

- The convection heat transfer coefficient between the glass cover and the ambient.

$$h_{g-amb}^{cv} = 5.7 + 3.8\ V_{wind} \quad (30)$$

- Coefficient of heat transfer by convection between the glass cover and the top protective glass.

$$h_{cv} = \frac{Nu_{air}\lambda_{air}}{e_{air}} \quad (31)$$

WhereNu_{air}, λ_{air}et e_{air} are the Nusselt number, the thermal conductivity of the air gap and the distance between the glass cover and the top protective glass. The Nusselt number was calculated using the Hollands formula [25].

$$Nu_{air} = 1 + \left[\left(\frac{Racos\gamma}{5830}\right)^{\frac{1}{3}} - 1\right]^{+}$$
$$+1.44\left[1 - \frac{1708}{Racos\gamma}\right]^{+} \times \left[1 - \frac{1708(sin1.8\gamma)^{1,6}}{Racos\gamma}\right] \quad (32)$$

The Rayleigh number of free convection heat transfer is given by equation 34.

$$R_a = \frac{g\beta_{air}(T_g-T_{g_1})e_{air}^3}{\mu_{air}^2 P_r} \quad (33)$$

Where $\beta_{air}, \mu_{air}, P_r, e_{air}$ and T_g-T_{g1} are the thermal expansion coefficient, dynamic air viscosity, the number of Prandtl, the thickness of the confined air layer, and the temperature difference between the glass cover and the top protective glass, respectively.

- The heat transfer coefficient of the fluid was defined from the Nusselt number of the fluid.

$$h_{ins-f}^{cv} = h_{p-f}^{cv} = \frac{Nu_f\lambda_f}{D_h} \quad (34)$$

$D_{h\mathrm{It}}$ is the equivalent diameter of the air flow channel.

The hydraulic diameter of the air duct without baffles is defined by formula 35 [28].

$$D_h = \frac{4(L\times\ell)}{2\times(L+\ell)} \quad (35)$$

In the case of an air flow channel with baffles, the hydraulic diameter is given by relationship 36 and is based on the methodology adopted by Bahria et al. [28].

$$D_h = \frac{4(L\times h-h_b e_b)}{2(L+h+h_b)} \quad (36)$$

What$h_b$is the height, and $e_b$what is the thickness of the baffles?

In a laminar air flow, viscous forces are dominant, and, consequently, Reynolds numbers are low, which are calculated using formula 37 [29].

$$R_e = \frac{mD_h}{\mu_f A_f} \quad (37)$$

WhereA_f,$m$andμ_f represent the air flow cross-section, the air mass flow rate and the air viscosity, respectively.

The Reynolds number delimits three classical flow regimes. In the case of laminar flow (R_e< 2300), the Nusselt number of the fluid is given by formula 38 [27].

$$N_{u_f} = 5.4 + \frac{0.00190\left[P_r R_e \frac{D_h}{L}\right]^{1.71}}{1+0.00563\left[P_r R_e \frac{D_h}{L}\right]^{1.17}} \quad (38)$$

- The coefficient of heat exchange by conduction between a solid layer $i$and another solid layer$j$is given by the following equation 39 [30].

$$h_{i-j}^{cd} = h_{j-i}^{cd} = \frac{1}{\frac{e_i}{\lambda_i}+\frac{e_j}{\lambda_j}} \quad (39)$$

The thermophysical properties of air vary linearly with temperature according to Ong's assumptions [31].

- Specific air heat:
$$C_f = 1.0057 + 0.000066(T_f - 27) \quad (40)$$

- Air density:
$$\rho_f = 1.1774 - 0.00359(T_f - 27) \quad (41)$$

- Thermal conductivity of air:
$$\lambda_f = 0.02624 + 0.0000758(T_f - 27) \quad (42)$$

- Dynamic air viscosity:
$$\mu_f = \left[1.983 + 0.00184(T_f - 27)\right] \times 10^{-5} \quad (43)$$

3.4. Performance Evaluation of the Hybrid PVT Air Flat-Plate Solar Collector

The assessment of energy performance is based on the first law of thermodynamics. Three efficiencies were used to

analyse the energy performance of the hybrid PVT air-flat plate collector [32-34].

- The electrical efficiency of PV solar cells is related to their operating temperature.

$$\eta_{el,pv} = \eta_{pv}^{ref}\beta\left[1 - \beta_{pv,ref}\left(T_{pv} - T_{pv}^{ref}\right)\right] \quad (44)$$

- The electrical power produced by the collector was calculated as follows:

$$P_{el,pv} = \eta_{el,pv} A_{pvt} G \quad (45)$$

- The useful thermal power of the hybrid PVT solar collector was calculated by using the product of mass flow, specific thermal capacity of air and the difference between outlet and inlet temperature.

$$P_{th} = m \times C_p \times (T_{out} - T_{in}) \quad (46)$$

- The efficiency of the hybrid PVT solar collector is calculated using equation 47.

$$\eta_{th} = \frac{P_{th}}{G \times A_{pvt}} \quad (47)$$

The total output power of the hybrid PVT solar collector is calculated using equation 48.

$$P_{tot} = P_{el} + P_{th} \quad (48)$$

- The overall efficiency of the hybrid PVT collector is calculated using equation 49.

$$\eta_{PVT} = \frac{E_{el} + E_{th}}{G \times A_{pvt}} = \eta_{el} + \eta_{th} \quad (49)$$

3.5. Exergy Performance Evaluation

The first law of thermodynamics only indicates the conservation of energy, i.e. the quantity of energy produced; it does not show whether the energy produced is of good quality or not. An approach that takes into account the quality of the energy produced is called exergy. Exergy analysis is based on the second law of thermodynamics. It represents the energy production capacity, i.e. the maximum amount of work produced. The exergy balance under dynamic conditions is expressed by equation 50 [35-37].

$$Ex_{in} = Ex_{el} + Ex_{th} + Ex_{dest} \quad (50)$$

Where Ex_{in},Ex_{th},Ex_{el}andEx_{dest} represent input, thermal, electrical and lost or destruction exergy, respectively.

The electrical and thermal exergy efficiency are defined by equations 51 and 52, respectively.

$$\eta_{x_{el}} = \frac{Ex_{el}}{E_{xin}} \quad (51)$$

$$\eta_{x_{th}} = \frac{Ex_{th}}{E_{xin}} \quad (52)$$

- The thermal exergy is calculated using equation 53.

$$Ex_{th} = mC_f\left[\left(T_f^{out} - T_f^{in}\right) - T_{amb}\, ln\left(\frac{T_f^{out}}{T_f^{in}}\right)\right] \quad (53)$$

- The electrical energy available is equal to the electrical energy produced by a hybrid PVT solar collector, since electrical energy can be completely transformed into work in any environment.

$$Ex_{el} = E_{el} \quad (54)$$

- The input exergy rate is calculated by equation 55.

$$Ex_{in} = \left(1 - \frac{4T_{amb}}{3T_{sun}} + \frac{1}{3}\left(\frac{T_{amb}}{T_{sun}}\right)^4\right) A_{pvt} G \quad (55)$$

Where T_{sun} (5800 K) represents the temperature at the surface of the sun, which is considered a black body.

The total exergy efficiency of the hybrid PVT solar collector is defined by equation 56.

$$\eta_{x_{pvt}} = \eta_{x_{th}} + \eta_{x_{el,pv}} \quad (56)$$

The destruction exergy of the system and the entropy production rate are determined by equations 57 and 58.

$$Ex_{dest} = Ex_{in} - Ex_{el} - Ex_{th} \quad (57)$$

$$S_g = \frac{Ex_{dest}}{T_{amb}} \quad (58)$$

4. Results and Discussion

In this section, the model is validated using experimental results from the literature and the energy and exergy performances of the hybrid PVT air collectors without and with baffles are compared with the numerical results obtained.

4.1. Numerical Solution Procedure

The resulting differential equations associated with the boundary conditions were solved numerically using the finite difference method. The implicit alternating directions scheme based on an implicit and explicit alternating directions fractional step scheme was used for the discretisation of the fluid convection and diffusion terms. On the solid layers of the hybrid PVT collector, the finite difference method with a simple implicit scheme was used. The discretised algebraic equations are written in the form of equation 59.

$$A_i \Phi_{i-1}^{k+1} + B_i \Phi_i^{k+1} + C_i \Phi_{i+1}^{k+1} = D_i \quad (59)$$

The discretized algebraic equations obtained were solved by the direct matrix inversion method of the Thomas algorithm. For the convergence criterion of the iterative process, the relative error on the dependent variables Φ between two successive iterations was taken to be less than 10^-6. Five different meshes in axial and radial direction, respectively, 82×73, 93×79, 114×86, 131×92, 139×99 nodes are chosen for mesh independence test with the air mass flow rate of 0.0096 kg/s, solar radiation intensity of 1000 W/m², air inlet temperature of 27 °C and wind speed of 1 m/s. The optical properties and thermophysical properties of the system are listed in Tables 1 and 2. Table 3 shows that the PV solar cell temperature and the air outlet temperature in the duct of the hybrid PVT flat-plate air collector were almost the same for all the nodes considered. Therefore, the node of size 82×73 was used in the present study in order to obtain accurate results with minimum computation time.

Table 1. Optical properties of the hybrid PVT solar collector [40, 41]

Optical properties	Values
Absorptivity of glass (α_g)	0.05
Glass emissivity (ε_g)	0.88
Transmissivity of glass (τ_g)	0.90
Absorptivity of PV cells (α_{pv})	0.95
Absorptivity of Tedlar (α_{td})	0.80
Absorber emissivity (ε_p)	0.95
Emissivity of insulation (ε_{ins})	0.90

4.2. Validation

The present mathematical model is validated by comparing simulated and experimental results with a root mean square percentage error (RMSE) defined by equation 60. [38, 39]

$$RMSE = \sqrt{\frac{\sum[100\times(X_{sim,i}-X_{exp,i})/X_{exp,i}]^2}{n}} \qquad (60)$$

With the number of experiments performed, the simulated data and the experimental data are the model was validated using experimental results obtained by Srimanickam et al. [7]. Figures 3 and 4 show good agreement between the experimental and simulated results.

4.3. Meteorological Data

The climatic conditions used were measured at the Solar Energy Laboratory on 16 March 2024 in Lomé, Togo, corresponding to the following geographical coordinates: latitude 6.13° and longitude 1.23°. The global solar radiation, the ambient temperature and the wind speed varying between 6:00 and 18:00 are represented in Figure 5 for an angle of inclination equal to the latitude of the site. In the present work, certain parameters were kept fixed: these are the inlet air mass flow rate fixed at 0.0096 kg/s, the inlet air temperature equal to the average ambient temperature and fixed at 27°C, and the wind speed at the surface of the PV module, which remains constantly stable at 1 m/s.

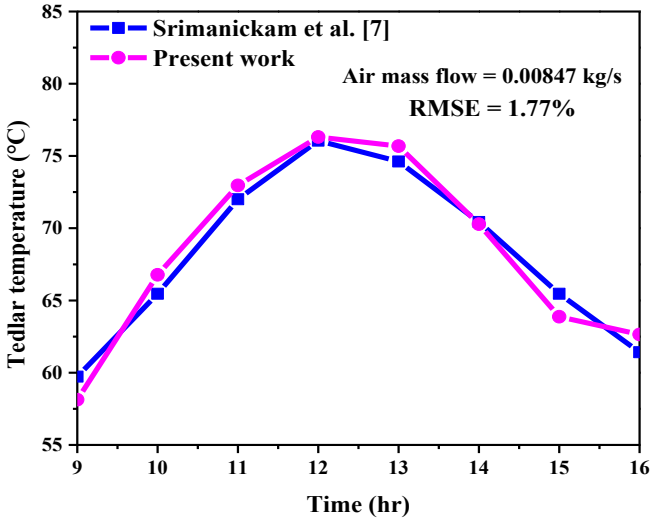

Fig. 3 Comparison of tedlar temperature

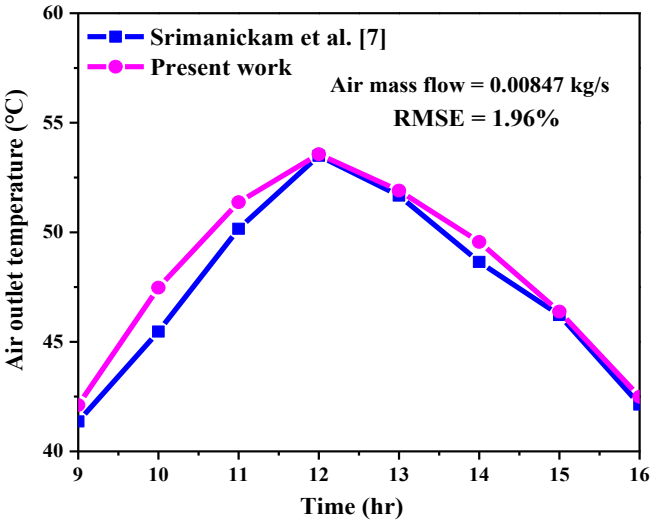

Fig. 4 Comparison of air outlet temperature

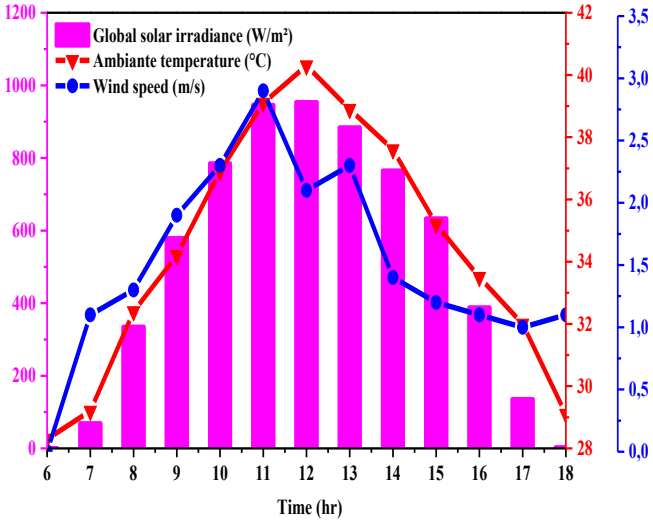

Fig. 5 Variations in global solar irradiance, ambient temperature and wind speed on 16 March 2024 in Lomé, Togo

Table 2. Thermophysical properties of the hybrid PVT solar collector [40, 42]

Layers	Dimensions (m)	k (W/m. K)	ρ (kg/m^3)	C (J/kg. K)
Glass	1.2×0.542×0.003	1.1	2700	840
Closed air	1.2×0.542×0.02	0.026	1.184	1007
PV cells	1.2×0.542×0.0003	0.036	2330	700
Tedlar	1.2×0.542×0.0005	0.2	1200	1250
Air	1.2×0.542×0.3	0.026	1.184	1007
Absorber	1.2×0.542×0.002	54	7833	465
Insulation	1.2×0.542×0.05	0.041	15	880

Table 3. Results of the mesh independence test for the hybrid PVT solar collector

Dimensions	82×73	93×79	114×86	131×92	139×99
T_{out} (°C)	40.70	40.14	40.25	40.30	40.72
T_{pv} (°C)	52.58	52.66	52.72	52.75	52.79
Time (s)	371	430	1184	1249	2322

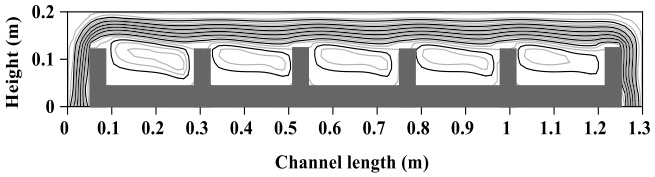

Fig. 6 Distribution of air streamlines of the hybrid PVT flat-plate collector with baffles

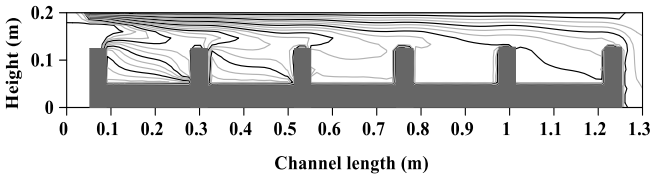

Fig. 7 Distribution of fluid isotherms in the air duct of the hybrid PVT flat-plate air collector with baffles

4.4. Analysis of Air Streamlines

Figure 6 shows the flow structure where the air is diverted towards the top and bottom walls with recirculation zones upstream and downstream of each baffle. One set of open lines runs in the upper section and another in the lower section of the air duct. The lines in the lower section bypass the baffles by wrapping around the microcells located around the ends of the baffles, thus preventing them from coming into contact with the baffles. Two forced flows that encourage convection at the top and bottom walls envelop these cells. The two sets of open lines merge in the right-hand bend of the air duct and flow towards the outlet. The coexistence of open lines and small cells indicates that the flow is by forced and natural convection. As the cells are very small, their intensity is very low and forced convection predominates. This flow structure will have a considerable influence on the distribution of the temperature field and will allow better mixing of the fluid, which will stimulate heat transfer.

4.5. Thermal Analysis of the Flat-Plate Hybrid PVT Air Collector

The distribution of isotherms is shown in Figure 7. The upper part of the air duct is occupied by parallel isotherms. This part of the cavity is the site of thermal stratification, as illustrated by the isothermal lines at this point. The narrowing of the isothermal lines near the top indicates good heat exchange due to the passage of fresh air. Exchange near the adiabatic underside of the cavity is improved by the presence of baffles that obstruct the airflow. The presence of the obstacles encourages air mixing and projects fresh air flow upwards, thus promoting the removal of heat from the upper face on which the heat flow is imposed. Distortions in the isothermal lines near the baffles are due to the injection of fresh air through these obstacles. The temperature of the fluid increases with its kinematic evolution in the upper and lower channels, thanks to its exchanges by convection with the absorber plate. Figures 8 and 9 show the PV solar cells temperature and the air outlet temperature for the PV module and the hybrid PVT flat-plate air collector with and without baffles, respectively. Under the same weather and operating conditions, the maximal temperature of the PV solar cells was 57.67°C for the hybrid PVT flat-plate air collector without baffles and 50.22°C for the hybrid PVT flat-plate air collector with baffles. The air temperature at the hybrid PVT flat-plate air collector outlet with baffles was 47.27°C and 44.45°C for the hybrid PVT flat-plate air collector without baffles under the same operating and weather conditions. This cooling method achieved a 7.45°C reduction in PV module temperature and a 2.82°C increase in duct outlet air temperature. These results clearly show that the addition of baffles in the air duct of the hybrid PVT flat-plate collector significantly reduced the temperature of the solar PV module by removing most of the heat at the back.

4.6. Energy Analysis of the Hybrid PVT air Collector

Figures 10 and 11 show the evolution of thermal and electrical powers of hybrid PVT collectors with or without baffles as a function of time. The maximal values for thermal and electrical power were 85.79 W and 168.77 W, respectively, for the hybrid PVT collector without baffles. For the PVT hybrid collector with baffles, they were 88.68 W and 195.96 W, respectively. The addition of the baffles in the air duct therefore improves thermal power by 27.19 W and electrical power by 2.89 W.

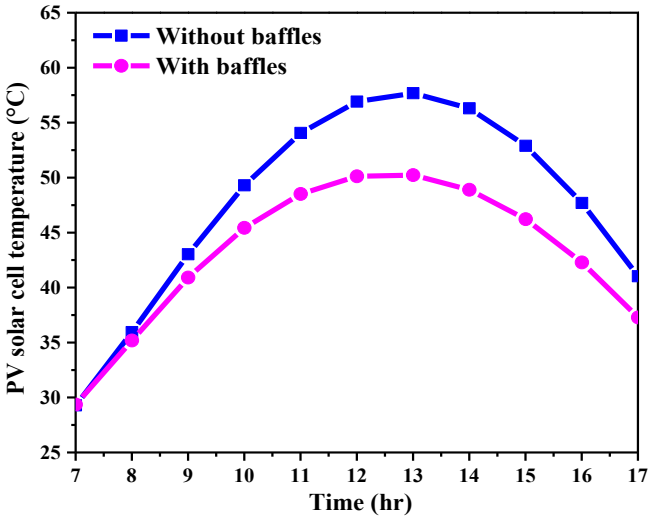

Fig. 8 Temperature variations of PV solar cells as a function of time

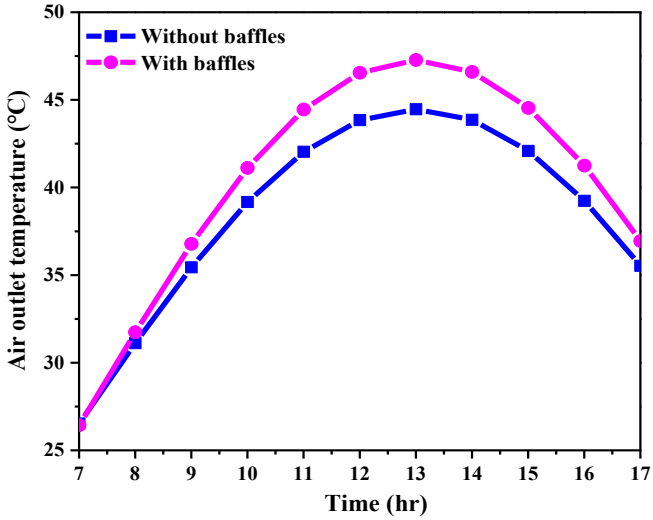

Fig. 9 Variations in air outlet temperatures as a function of time

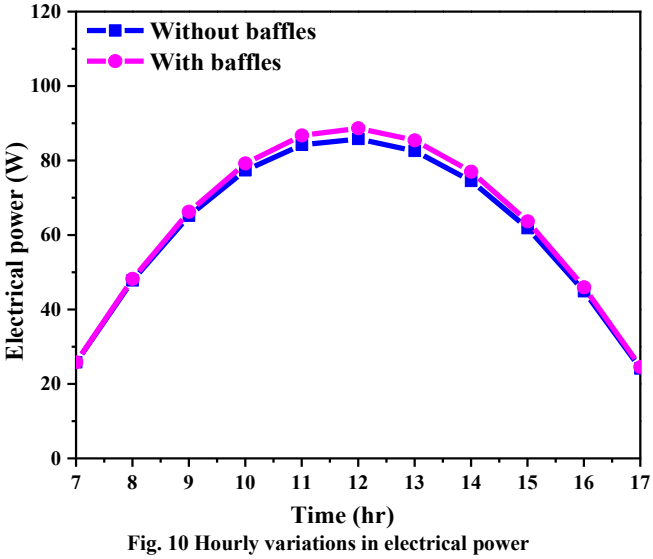

Fig. 10 Hourly variations in electrical power

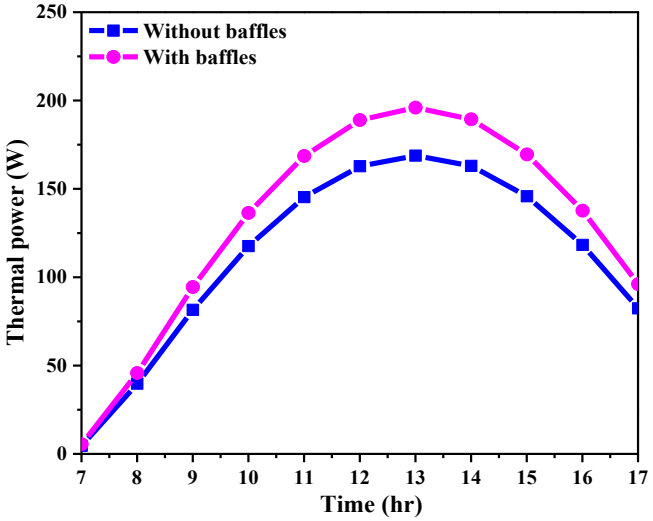

Fig. 11 Hourly variations in thermal power

Figures 12 and 13 show the hourly evolution of the electrical and thermal efficiencies of the two configurations. For the hybrid PVT flat-plate air collector without baffles, the minimal electrical efficiency and maximal thermal efficiency were 13.74% and 46.59% respectively, while for the hybrid PVT flat-plate air collector with baffles, they were 14.22% and 60.64% at 13:00.

The overall efficiency as a function of time and the average daily efficiency are shown in Figures 14 and 15 for the two configurations. Figure 14 shows that the maximal overall efficiency of the hybrid PVT air solar collector without baffles was 60.63% and 74.87% for a hybrid PVT air solar collector with baffles at 13:00.

Figure 15 illustrated that the average thermal efficiency was 32.36% and 40.18% for the hybrid PVT air collector without baffles and the hybrid PVT air hybrid collector with baffles, respectively.

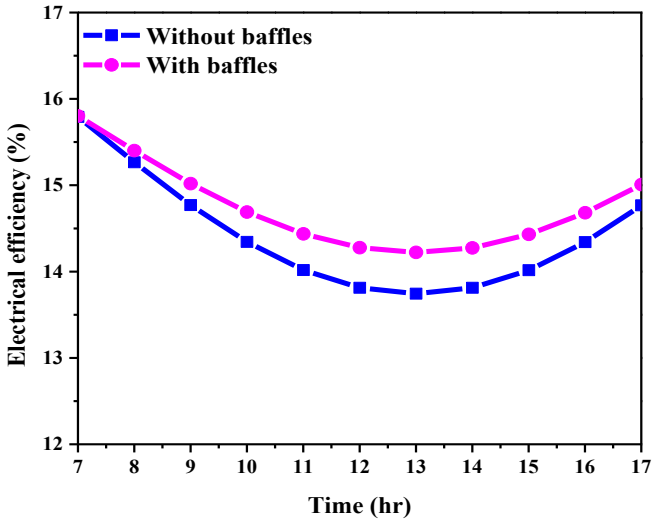

Fig. 12 Hourly variations in electrical efficiency

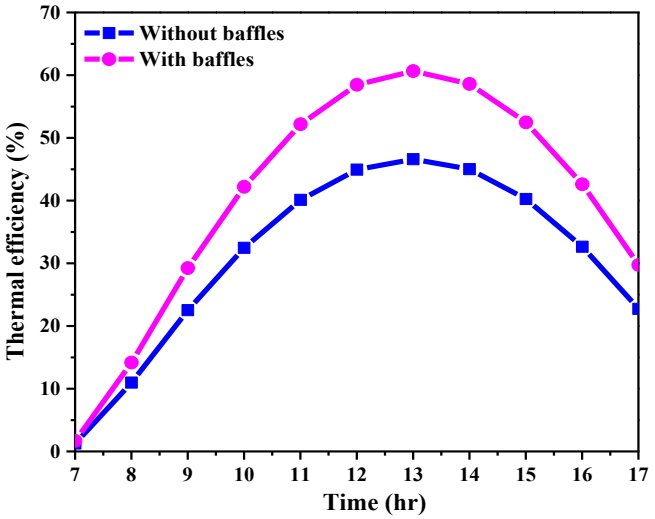

Fig. 13 Hourly variations in thermal efficiency

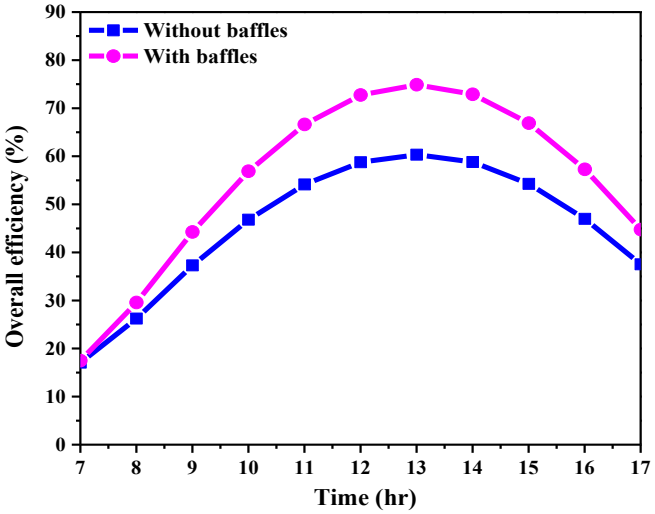

Fig. 14 Variations in overall efficiency as a function of time

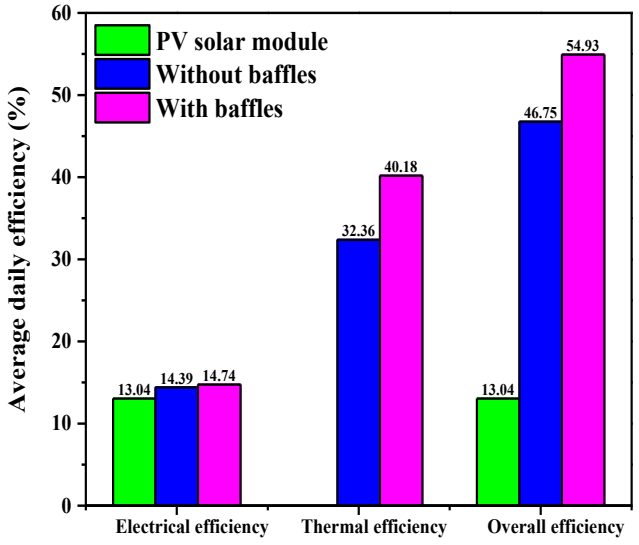

Fig. 15 Daily average electrical, thermal and overall efficiencies

Similarly, the average electrical efficiency was 13.04%, 14.39% and 14.74% respectively, for the PV module, the hybrid PVT air collector without baffles and the hybrid PVT air collector with baffles. The average overall efficiency was 46.75% for the hybrid PVT air collector without baffles and 54.93% for the PVT air collector with baffles.

Figure 16 shows the daily energy production. The average overall energy output was 1.78 kWh for the hybrid PVT air collector without baffles, compared with 1.93 kWh for the hybrid PVT air collector with baffles. The average daily electrical energy was 0.58 kWh, 0.61 kWh, and 0.63 kWh for the PV module, the hybrid PVT air collector without baffles, and the hybrid PVT air collector with baffles. On the other hand, the average daily thermal energy was 1.17 kWh and 1.30 kWh for the hybrid PVT air collector without baffles and with baffles, respectively.

4.7. Analysis of Exergetic Performance

Figures 17 and 18 illustrate the variations in electrical exergetic efficiency and thermal exergetic efficiency as a function of time of the hybrid PVT air solar collector with and without baffles.

Figure 17 shows that the electrical efficiency is identical to the electrical exergy efficiency by virtue of the principle that electrical energy is totally transformed into work according to the second law of thermodynamics. In fact, the minimum electrical exergy efficiencies of the hybrid PVT air collector without baffles and the hybrid PVT air collector with baffles were 14.32% and 15.28% respectively, at 13:00.

Maximizing the output power of the hybrid PVT flat-plate air solar collector is similar to the minimization of entropy generation. Entropy production is a parameter used to show the irreversibility of a solar system. In this section, we studied the effect of adding baffles to one of the two configurations on thermal entropy production.

Figure 18 shows that the thermal exergy efficiencies of the two configurations began to increase as the ambient temperature and solar radiation increased; this confirms the second law of thermodynamics. The maximal daily thermal exergy efficiencies of the hybrid PVT flat-plate air collector without baffles and the hybrid PVT flat-plate air collector with baffles were 1.43% and 1.61% at 13:00, respectively. The contribution of thermal exergetic efficiency is therefore lower compared to electrical exergetic efficiency.

The changes in overall exergy efficiency and entropy production over the day are shown in Figures 19 and 20. The overall exergy efficiency was 15.76% and 16.90% for the flat-plate hybrid PVT air collector without baffles and the flat-plate hybrid PVT air collector with baffles, respectively. The results in Figure 20 showed that the flat-plate hybrid PVT air collector with baffles produced the maximal value of entropy

of 1.60 W/K, while the flat plate hybrid PVT air collector without baffles produced only 1.65 W/K at 12:00. This improvement can be explained by:

- The increase in the heat exchange area, which represented 8% of the total surface area of the heat exchanger, contributed to the improvement in the convection coefficient between the absorbent plate and the flowing air.
- The presence of the baffles changed the nature of the flow by creating vortices, which promoted heat exchange.

4.8. Analysis of Improved Efficiency and Heat Transfer

The hybrid PVT flat plate air collector with baffles kept the temperature of the PV solar module permanently lower than that of the hybrid PVT flat plate air collector without baffles.

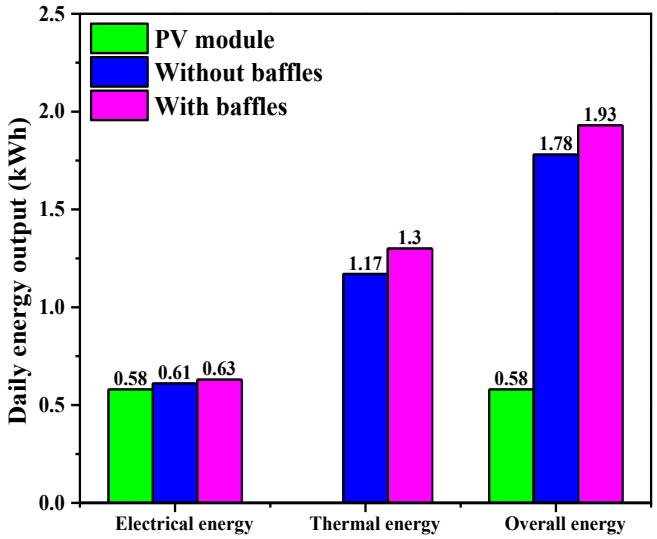

Fig. 16 Average daily energy output

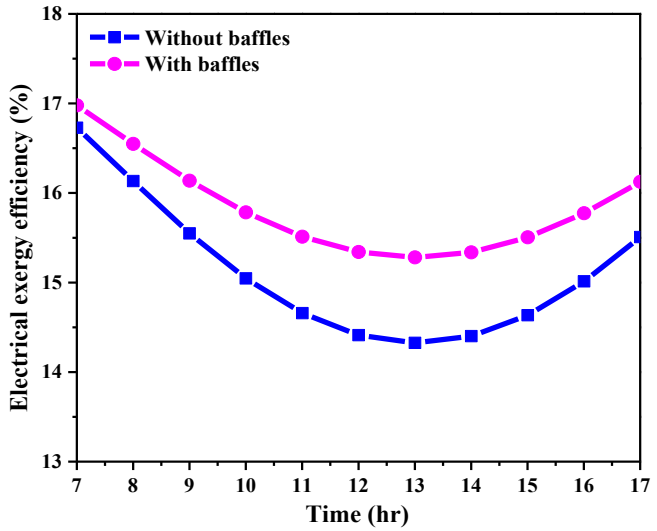

Fig. 17 Variations in electrical exergetic efficiency as a function of time

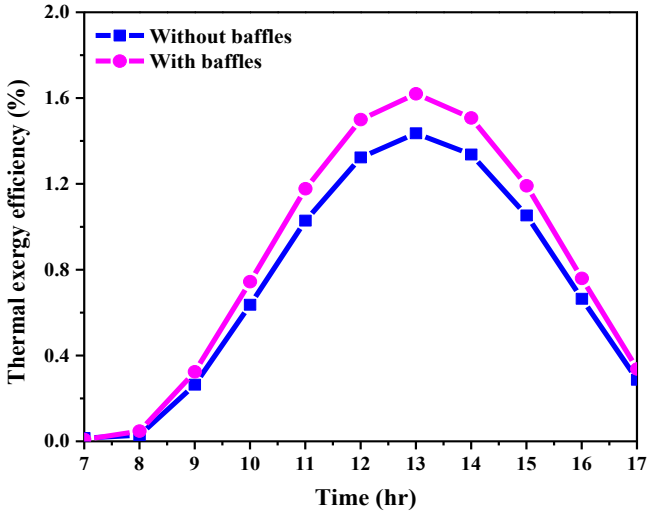

Fig. 18 Variations in thermal exergetic efficiency as a function of time

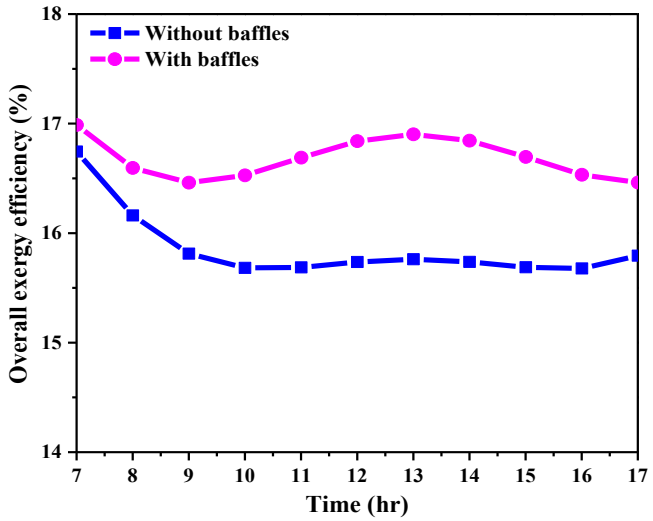

Fig. 19 Variation in overall exergetic efficiency as a function of time

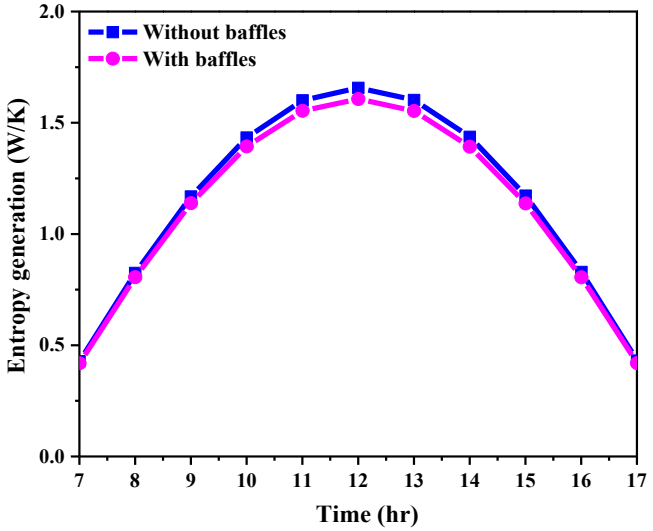

Fig. 20 Entropy production as a function of time

The baffles introduced into the air duct therefore improved heat removal from the PV solar module. Comparative analysis of the thermal and electrical efficiency of the hybrid PVT flat plate air collector with baffles showed a significant improvement in electrical efficiency. The average electrical efficiency of the PV module increased from 13.04% to 14.39% for the hybrid PVT flat-plate air collector without baffles and from 13.04% to 14.74% for the hybrid PVT flat-plate air collector with baffles. This represents a 1.70% difference in electrical efficiency and a maximum overall efficiency gain of 40.18%. A 13.04% improvement in electrical efficiency over the PV module and a 2.43% improvement over the hybrid PVT flat plate air collector without rectangular baffles.

The results obtained are better than those of An et al. [20], who obtained a 1.76% improvement in electrical efficiency in a numerical and experimental study compared to the hybrid PVT flat plate air collector without triangular baffles. Similarly, the results obtained are also better than those obtained by Zine et al. [23], who obtained a 22% improvement in overall efficiency compared to a hybrid PVT collector without baffles in the absorber. Previous studies have also obtained similar results, proving that the addition of baffles can reduce the temperature of the solar PV module, thus improving its electrical efficiency. However, this result depends on the configuration, shape and number of baffles.

5. Conclusion

This paper has developed a numerical model of the hybrid PVT flat plate air collector with baffles from the basic equations governing the air flow and the energy balance. The algebraic equations obtained after discretization were solved by Thomas' algorithm and validated. The daily energy performance of the hybrid PVT flat-plate air collector with and without chicanes was studied. The temperature of the PV solar module decreased from 57.67°C to 50.22°C when baffles were added in the air duct, while the temperature of the air at the outlet increased from 44.45°C to 47.27°C. The average daily thermal efficiency was 32.36% for the hybrid PVT flat-plate air collector without baffles and 40.18% for the hybrid PVT flat-plate air collector with baffles. The average electrical efficiency was 13.04%, 14.39% and 14.74% respectively, for the PV module, the hybrid PVT flat-plate air collector without baffles and the hybrid PVT flat-plate air collector with baffles. The maximal overall exergy efficiency is 15.76% for the hybrid PVT flat-plate air collector without baffles and 16.90% for the hybrid PVT flat-plate air collector with baffles. The maximum value of entropy production for the hybrid PVT flat-plate air collector without baffles was 1.65 W/K, while the hybrid PVT flat-plate air collector with baffles produced only 1.60 W/K. The addition of baffles in the air duct has resulted in a reduction in the temperature of the solar photovoltaic module and an increase in the temperature of the air at the outlet of the hybrid PVT flat-plate air collector, thereby improving electrical efficiency. The flat-plate hybrid PVT air collector with baffles showed better daily energy performance, confirming the importance of adding baffles in cooling PV solar modules. Although trends in electrical efficiency may vary, the overall efficiency observed highlights the potential of baffles to optimise electrical performance. By keeping the operating temperature of the PV solar module lower through heat removal, the baffles prevented degradation of the PV solar cells, thereby contributing to increased electricity production. In the future, an experimental study will be carried out under the actual operating conditions of the hybrid PVT flat plate air collector designed to complement the numerical study carried out in this paper. The effect of mass flow rate and pressure drop on performance will be analysed in turbulent flow.

Funding Statement

The work was supported by funding from the World Bank for the project "Centre d'Excellence Régional pour la Maîtrise de l'Electricité (CERME)" of the University of Lomé, Togo (Crédit IDA 6512-TG; Don IDA 536IDA).

Acknowledgments

The authors gratefully acknowledge the support of all CERME and LES (Solar Energy Laboratory) staff for their assistance.

Authors Contributions

Yao Kombate and Kokou N'wuitcha conceived and designed the research. Yao Kombate and Kokou N'wuitcha carried out the numerical simulation. Yao Kombate wrote the manuscript and original draft. Yendouban Kolani and Komlan Déla Donald Aoukou contributed numerical tools and reviewed the manuscript. Koffi Gagnon Apedanou and Bernard Obese analyzed data and reviewed the manuscript. All authors read and approved the manuscript.

References

[1] S.C. Bhatia, *Advanced Renewable Energy Systems*, Woodhead Publishing India Pvt. Ltd., 2025. [Google Scholar] [Publisher Link]

[2] Basant Agrawal, and Gopal Nath Tiwari, *Building Integrated Photovoltaic Thermal Systems: for Sustainable Developments*, Royal Society of Chemistry Energy Series, RCS Publishing, 2010. [CrossRef] [Google Scholar] [Publisher Link]

[3] Karunesh Kant et al., "Thermal Response of Poly-Crystalline Silicon Photovoltaic Panels: Numerical Simulation and Experimental Study, *Solar Energy*, vol. 134, pp. 147-155, 2016. [CrossRef] [Google Scholar] [Publisher Link]

[4] Socrates Kaplanis, and Eleni Kaplani, "A New Dynamic Model to Predict Transient and Steady State PV Temperatures Taking into Account the Environmental Conditions," *Energies*, vol. 12, no. 1, pp. 1-17, 2019. [CrossRef] [Google Scholar] [Publisher Link]

[5] Ioan Sarbu, and Calin Sebarchievici, *Solar Heating and Cooling Systems: Fundamentals, Experiments and Applications*, Academic Press, 2017. [Publisher Link]

[6] Zain Ul Abdin, and Ahmed Rachid, "A Survey on Applications of Hybrid PV/T Panels," *Energies*, vol. 14, no. 4, pp. 1-23, 2021. [CrossRef] [Google Scholar] [Publisher Link]

[7] B. Srimanickam, M.M. Vijayalakshmi, and E. Natarajan, "Energy and Exergy Efficiency of Flat Plate PVT Collector with Forced Convection," *Journal of Testing and Evaluation*, vol. 46, no. 2, pp. 783-797, 2018. [CrossRef] [Google Scholar] [Publisher Link]

[8] Omer Khalil Ahmed, and Zala Aziz Mohammed, "Experimental Investigation of PV/Thermal Collector with Theoretical Analysis," *Renewable Energy Focus*, vol. 27, pp. 67-77, 2018. [CrossRef] [Google Scholar] [Publisher Link]

[9] T.A. Tripty, and R. Nasrin, "Efficiency Upgrading of Solar PVT Finned Hybrid System in Bangladesh: Flow Rate and Temperature Influences," *Heliyon*, vol. 10, no. 7, pp. 1-23, 2024. [CrossRef] [Google Scholar] [Publisher Link]

[10] Rajamohan Ganesan et al., "Experimental Study of Natural Convective Heat Transfer Cooling System in Solar Panels," *AIP Conference Proceedings: Industrial, Mechanical and Electrical Engineering*, Brunei, pp. 1-6, 2022. [CrossRef] [Google Scholar] [Publisher Link]

[11] Ali Basem et al., "Experimental Study on the Various Varieties of Photovoltaic Panels (PVs) Cooling Systems to Increase their Electrical Efficiency," *PLoS ONE*, vol. 19, no. 9, pp. 1-24, 2024. [CrossRef] [Google Scholar] [Publisher Link]

[12] Ahssan M.A. Alshibil, Piroska Vig, and Istvan Farkas, "Performance Enhancement Attempts on the Photovoltaic/Thermal Module and the Sustainability Achievements: A Review," *Energy*, vol. 304, pp. 1-28, 2024. [CrossRef] [Google Scholar] [Publisher Link]

[13] Zhang Rundong et al., "Numerical Model and Efficiency Analysis of Finned Staggered Solar PV/T Air Collector," *Thermal Science*, vol. 28, no. 2 Part A, pp. 941-960, 2024. [CrossRef] [Google Scholar] [Publisher Link]

[14] Ziqiang Wang et al., "Numerical Investigation of Innovative Photovoltaic-Thermal (PVT) Collector Designs for Electrical and Thermal Enhancement," *Energies*, vol. 17, no. 10, pp. 1-27, 2024. [CrossRef] [Google Scholar] [Publisher Link]

[15] Seong-Bhin Kim et al., "Experimental Performance Evaluation of Air-Based Photovoltaic-Thermal Collector with Rectangular Turbulators and Longitudinal Fins," *Energy Reports*, vol. 12, pp. 1315-1324, 2024. [CrossRef] [Google Scholar] [Publisher Link]

[16] Zhang Genge et al., "Solar Photovoltaic Surface Cooling Using Hybrid Solar Chimney-Collector with Wavy Fins," *Journal of Advanced Research in Numerical Heat Transfer*, vol. 22, no. 1, pp. 46-58, 2024. [CrossRef] [Google Scholar] [Publisher Link]

[17] Fatih Bayrak, Hakan F. Oztop, and Fatih Selimefendigil, "Effects of Different Fin Parameters on Temperature and Efficiency for Cooling of Photovoltaic Panels Under Natural Convection," *Solar Energy*, vol. 188, pp. 484-494, 2019. [CrossRef] [Google Scholar] [Publisher Link]

[18] Sourav Khanna, K.S. Reddy, and Tapas K. Mallick, "Performance Analysis of Tilted Photovoltaic System Integrated with Phase Change Material Under Varying Operating Conditions," *Energy*, vol. 133, pp. 887-899, 2017. [CrossRef] [Google Scholar] [Publisher Link]

[19] Jong-Gwon Ahn et al., "Simulation and Performance Analysis of Air-Type PVT Collector with Interspaced Baffle-PV Cell Design," *Energies*, vol. 14, no. 17, pp. 1-12, 2021. [CrossRef] [Google Scholar] [Publisher Link]

[20] Byeong-Hwa An, Kwang-Hwan Choi, and Hwi-Ung Choi, "Influence of Triangle-Shaped Obstacles on the Energy and Exergy Performance of an Air-Cooled Photovoltaic Thermal (PVT) Collector," *Sustainability*, vol. 14, no. 20, pp. 1-19, 2022. [CrossRef] [Google Scholar] [Publisher Link]

[21] Ji-Suk Yu, Jin-Hee Kim, and Jun-Tae Kim, "Effect of Triangular Baffle Arrangement on Heat Transfer Enhancement of Air-Type PVT Collector," *Sustainability*, vol. 12, no. 18, pp. 1-13, 2020. [CrossRef] [Google Scholar] [Publisher Link]

[22] B. Srimanickam, and A. Saranya, "Thermal Performance of Single Glazing Flat Plate Photovoltaic Thermal Hybrid System with Various Air Channels," *Journal of Testing and Evaluation*, vol. 49, no. 3, pp. 2119-2150, 2021. [CrossRef] [Google Scholar] [Publisher Link]

[23] Saadi Zine et al., "Experimental Study of Hybrid Photovoltaic (PV/T) Thermal Solar Collector with Air Cooling for Domestic Use: A Thermal and Electrical Performances Evaluation," *Journal of Advanced Research in Fluid Mechanics and Thermal Sciences*, vol. 116, no. 1, pp. 170-183, 2024. [CrossRef] [Google Scholar] [Publisher Link]

[24] Xiaofei Hou, "*Numerical Modeling of Complex Heat Transfer Phenomena in Cooling Applications*," Doctoral Thesis, Polytechnic University of Catalonia, 2015. [CrossRef] [Google Scholar] [Publisher Link]

[25] K.G.T. Hollands et al., "Free Convective Heat Transfer across Inclined Air Layers," *Journal of Heat Transfer*, vol. 98, no. 2, pp. 189-193, 1976. [CrossRef] [Google Scholar] [Publisher Link]

[26] Theodore L. Bergma et al., *Fundamentals of Heat and Mass Transfer*, 8th ed., John Wiley & Sons, Inc., 2018. [Google Scholar] [Publisher Link]

[27] John A. Duffie, and William A. Beckman, *Solar Engineering of Thermal Processes*, John Wiley and Sons, 2013. [CrossRef] [Google Scholar] [Publisher Link]

[28] Sofiane Bahria, and Madjid Amirat, "Influence of the Addition of Longitudinal Baffles on the Performance of a Flat Air Solar Collector," *Journal of Renewable Energies*, vol. 16, no. 1, pp. 51-63, 2013. [CrossRef] [Google Scholar] [Publisher Link]

[29] Afroza Nahar et al., "Numerical Investigation on the Effect of Different Parameters in Enhancing Heat Transfer Performance of Photovoltaic Thermal Systems," *Renewable Energy*, vol. 132, pp. 284-295, 2019. [CrossRef] [Google Scholar] [Publisher Link]

[30] Chaimae El Fouas et al., "Numerical and Parametric Analysis for Enhancing Performances of Water Photovoltaic/Thermal System," *Applied Sciences*, vol. 12, no. 2, pp. 1-17, 2022. [CrossRef] [Google Scholar] [Publisher Link]

[31] K.S. Ong, "Thermal Performance of Solar Air Heaters: Mathematical Model and Solution Procedure," *Solar Energy*, vol. 55, no. 2, pp. 93-109, 1995. [CrossRef] [Google Scholar] [Publisher Link]

[32] E. Skoplaki, and, J.A. Palyvos, "On the Temperature Dependence of Photovoltaic Module Electrical Performance: A Review of Efficiency/Power Correlations," *Solar Energy*, vol. 83, no. 5, pp. 614-624, 2009. [CrossRef] [Google Scholar] [Publisher Link]

[33] T.T. Chow, "A Review on Photovoltaic/Thermal Hybrid Solar Technology," *Applied Energy*, vol. 87, no. 2, pp. 365-379, 2010. [CrossRef] [Google Scholar] [Publisher Link]

[34] Soteris A. Kalogirou, *Solar Energy Engineering: Processes and Systems*," 2nd ed., Academic Press, 2014. [Google Scholar] [Publisher Link]

[35] Soteris A. Kalogirou, "Solar Thermal Collectors and Applications," *Progress in Energy and Combustion Science*, vol. 30, no. 3, pp. 231-295, 2004. [CrossRef] [Google Scholar] [Publisher Link]

[36] Seyed Reza Maadi et al., "Characterization of PVT Systems Equipped with Nanofluids-Based Collector from Entropy Generation," *Energy Conversion and Management*, vol. 150, pp. 515-531, 2017. [CrossRef] [Google Scholar] [Publisher Link]

[37] Arash Kazemian et al., "Energy, Exergy and Environmental Analysis of Glazed and Unglazed PVT System Integrated with Phase Change Material: An Experimental Approach," *Solar Energy*, vol. 201, pp. 178-189, 2020. [CrossRef] [Google Scholar] [Publisher Link]

[38] Arvind Tiwari, and, M.S. Sodha, "Performance Evaluation of Solar PV/T System: An Experimental Validation," *Solar Energy*, vol. 80, no. 7, pp. 751-759, 2006. [CrossRef] [Google Scholar] [Publisher Link]

[39] F. Sobhnamayan et al., "Optimization of a Solar Photovoltaic Thermal (PV/T) Water Collector Based on Exergy Concept," *Renewable Energy*, vol. 68, pp. 356-365, 2014. [CrossRef] [Google Scholar] [Publisher Link]

[40] Arvind Tiwari, and M.S. Sodha, "Parametric Study of Various Configurations of Hybrid PV/Thermal Air Collector: Experimental Validation of Theoretical Model," *Solar Energy Materials and Solar Cells*, vol. 91, no. 1, pp. 17-28, 2007. [CrossRef] [Google Scholar] [Publisher Link]

[41] Mohammed Mossad Hegazy et al., "Comparative Study of Three Different Designs of a Hybrid PV/T Double-Pass Finned Plate Solar Air Heater," *Environmental Science and Pollution Research*, vol. 27, no. 26, pp. 32270-32282, 2020. [CrossRef] [Google Scholar] [Publisher Link]

[42] M. Lyes et al., "Effect of Air Channel Depth and Mass Flow Rate on the Efficiency of Hybrid Thermal - Photovoltaic Sensor," *The International Journal of Multiphysics*, vol. 12, no. 2, pp. 147-168, 2018. [Google Scholar] [Publisher Link]